Supporting Information for

Absorbent filaments from cellulose nanofibril hydrogels through continuous coaxial wet-spinning

Meri J. Lundahl[*1], Ville Klar[2], Rubina Ajdary[1], Nicholas Norberg[3], Mariko Ago[1], Ana Gisela Cunha[1], Orlando J. Rojas*[*1]*

[1]Department of Bioproducts and Biosystems, Aalto University, Espoo, P.O. Box 16300, 00076 Aalto, Finland

[2]Department of Mechanical Engineering, Aalto University, Espoo, P.O. Box 14100, 00076 Aalto, Finland.

[3]PANalytical B.V., Almelo, The Netherlands.

* E-mail: meri.lundahl@aalto.fi (M.J.L.), Phone: +358 40 526 0787.

* E-mail: orlando.rojas@aalto.fi (O.J.R.), Phone: +358 50 512 4227.

This *Supporting Information* document contains 20 pages with 8 tables and 4 figures along with discussion organized in sections:

1. Spinning conditions for filaments prepared for different experiments
2. Effect of drawing on absorbent filaments with CNF and CA
3. Filament crystallinity
4. Effect of the shell material and coagulation system on filament physical-mechanical properties
5. Filament interactions with water
6. Effect of core/shell system on spinnability

1. SPINNING CONDITIONS FOR FILAMENTS PREPARED FOR DIFFERENT EXPERIMENTS

The spinning conditions varied between different sets of experiments for several reasons. For example, as the rheological nature of GG and CA differ,[1] different solids contents and extrusion speeds were required to obtain suitable flow behavior for core/shell wet-spinning (Table S1). Moreover, when optimizing the production rate (Table S2) and water absorption (Table S3), achieving the respective properties were prioritized instead of comparability with the standard samples. Tables S1 and S2 identify the spinning conditions used for the sample preparation and the determination of the maximum production rate, respectively. Table S3 specifies the conditions employed to spin absorbent filaments of CNF and CA, which were also used to study the effect of drawing, which will be discussed in the following section. These samples were prepared with an earlier iteration of the core/shell wet-spinning line (smaller winder and different needle size).

Table S1. Spinning conditions used for standard sample preparation.

	Core	Shell		Control
	CNF, 1.5 wt.% in water	GG, 1 wt.% in water	CA, 15 wt.% in acetone	GG only, 1 wt.% in water
Needle diameter (mm)	0.69 (outer 1.07)	1.80	1.80	0.69
Needle length (cm)	4.7	3.5	3.5	4.7
Volumetric extrusion speed (ml/min)	3.0	1.0	0.3	3.0
Extrusion speed (m/min)	8.0	0.6	0.2	8.0
Wall shear rate[1] (s^{-1})	2800	300	50	2600
Immersion time in	5 min in ethanol	5 min in	5 min in ethanol	5 min in acetone

coagulant	(with CA/GG) or acetone (with GG)	ethanol	or aeetone	
Winder diameter (cm)	22	22	22	22

Table S2. Spinning conditions for CNF/CA core/shell filaments prepared with prototype spinning line for speed optimization.

	CNF/CA		CNF/GG	
	CNF core, 1 wt.% in water	CA shell, 15 wt.% in acetone	CNF core 1.5 wt.% in water	GG shell, 1 wt.% in water
Needle diameter (mm)	0.84 (outer 1.27)	2.16	0.69 (outer 1.07)	1.80
Needle length (cm)	4.7	3.5	4.7	3.5
Volumetric extrusion speed (ml/min)	6.0	0.3	3.0	1.0
Extrusion speed (m/min)	11	0.13	8.121	0.546
Travel distance in coagulant	95 cm in 1:1 water-ethanol	95 cm in 1:1 water-ethanol	24 cm in acetone	24 cm in acetone
Winding speed (m/min)	33	33	1.2	1.2
Winder diameter (cm)	22	22	22	22

Table S3. Spinning conditions for CNF/CA core/shell filaments prepared for drawing and water absorption studies.

	CNF/CA		Control
	CNF core, 1 wt.% in water	CA shell, 15 wt.% in acetone	CA only, 15 wt.% in acetone
Needle diameter (mm)	0.88 (outer 1.25)	2.00	0.88
Needle length (cm)	6.4	3.7	6.4
Volumetric extrusion speed (ml/min)	1.0	0.1	0.05
Extrusion speed (m/min)	1.64	0.05	0.08
Wall shear rate[1] (s^{-1})	1100	14	12
Coagulation distance in water (cm)	33	33	26
Winder diameter (cm)	6	6	6

2. EFFECT OF DRAWING ON ABSORBENT FILAMENTS WITH CNF AND CA

The extension rate applied on the filament in the bath was controlled by varying the winding speed according to Table S4. The extension rate $\dot{\varepsilon}_{applied}$ was quantified by Equation S1:

$$\dot{\varepsilon}_{applied} = \left(\frac{v_{winder}}{v_{needle}} - 1\right)\frac{v_{winder}+v_{needle}}{2\,L_{bath}} \quad \text{(S1)}$$

where v_{needle} is the extrusion speed of the dope, v_{winder} is the winding speed and L_{bath} is the coagulation distance (i.e., the distance a filament element travels in the coagulation bath). Thus, v_{winder}/v_{needle} corresponds to the drawing ratio (DR) and $(v_{winder}+v_{needle})/2$ to the average speed of a filament element during the coagulation.

Table S4. Drawing ratios (DR) used for spinning core/shell filaments along with the corresponding extension rates and winding speeds.

CNF DR[a]	CNF extension rate (s^{-1})	CA DR[a]	CA extension rate (s^{-1})	Winding speed (m/min)
1	no extension	32	1.3	1.66
5	1	159	33.4	8.32
9	3.4	287	108.5	14.97
Control (CA only)	no CNF	32	2.1	2.65[b]

[a] Ratio of winding speed to extrusion speed, both in m/min.

[b] Higher winding speeds led to frequent breaking of the filament.

The core/shell spinning system enabled clearly higher DR and extension rates than applied in CNF wet-spinning previously. Previous efforts to stretch CNF are compiled in Table S5 along with the present study. Interestingly, in combination with the CNF core, CA could be drawn to an even larger extent than CA alone (Table S4). This observation suggests synergies between both components. The physical and mechanical properties of the CNF/CA filaments with varying DR are presented in Table S6.

Table S5. Drawing methods and respective ratios reported for cellulose nanofibrils (CNF) as well as the obtained orientation (reported by given parameters), Young's modulus and tensile strength for drawn filaments. The data include values from the present work.

Material	Draw method	DR[c]	Process speed, m/min	Extension rate, s^{-1}	Orientation	Young's modulus (increase)[g]	Tensile strength (increase)[g]	Ref.
Carboxy-methylated CNF filament	Flow focusing	1.15	0.84	n.a.[d]	0.50[e]	18 GPa (41%)	445 MPa (51%)	2
TEMPO[a]-oxidized CNF filament	Drawing in water	1.3	5×10^{-4} - 5×10^{-3}	$8x10^{-5}$ - $8x10^{-4}$	0.57[e] 83%[f]	33.7 GPa (311%)	289 MPa (145%)	3
TEMPO[a]-oxidized CNF filament	Drawing wet in air	1.1	n.a.[d]	n.a.[d]	73%[f]	23.9 GPa (42%)	294 MPa (18%)	4
TEMPO[a]-oxidized CNF and cationic polymer filament	IPC[b] spinning	1.2	n.a.[d]	$7x10^{-4}$	0.49[e] 79%[f]	20 GPa (33%)	250 MPa (26%)	5
TEMPO[a]-oxidized bacterial CNF filament	Drawing in water-acetone	1.2	8×10^{-4}	$2x10^{-4}$	0.67[e] 72%[f]	16.4 GPa (37%)	249 MPa (27%)	6
Unmodified CNF filament	Dry-spinning	1.7	660	n.a.[d]	n.a.[d]	n.a.[d]	220 MPa (52%)	7
Bacterial CNF array/tube	Stretching wet in air	1.2	3×10^{-5}	$2x10^{-5}$	68-71%[f]	13-17 GPa (54-63%)	230-260 MPa (46-48%)	8,9
PEG-grafted CNF hydrogel	Stretching wet in air	1.4	10^{-3}	$3x10^{-4}$	86%[f]	32.3 GPa (405%)	576 MPa (162%)	10
TEMPO[a]-oxidized CNF hydrogel	Stretching wet in air	1.6	n.a.[d]	$8x10^{-3}$	0.56[e] 81.7%[f]	33.3 GPa (223%)	397 MPa (115%)	11
TEMPO[a]-oxidized CNF hydrogel	Stretching wet in air	1.3	0.01	$2x10^{-3}$	n.a.[d]	46.6 GPa (352%)	474 MPa (37%)	12
Present work: Unmodified CNF filament	Core/shell spinning	5	8.32	1	0.23[e] 32%[f]	0.6 GPa (56%)	15 MPa (54%)	

[a] 2,2,6,6-Tetramethylpiperidine 1-oxyl

[b] Interfacial polyelectrolyte complexation

[c] Drawing ratio; i.e., ratio of the stretched film/filament length to unstretched; i.e. DR = 1 signifies no draw, DR < 1 negative draw or DR > 1 positive draw.

[d] Not available

[e] Herman's orientation parameter

[f] Degree of orientation

[g] improvement in % with respect to similar material prepared without drawing

Table S6. Physical and mechanical properties of CNF/CA filaments before and after CA removal (i.e., with and without CA) along with different drawing ratios (DR) of CNF. Error margins are defined as the standard deviation divided by the square root of the sample size (5 specimens). Spinning conditions: Tables S3, S4

	With CA			Without CA			CA only
CNF DR[a]	1	5	9	1	5	9	32[d]
Apparent thickness, µm	36.0±2.7	13.0±0.5	9.0±0.8	16.1±1.4	7.5±0.5	7.7±0.3	30.8±2.4
Apparent width, µm[b]	1078±75	584±31	259±18	1034±36	300±31	186±21	58±5
Apparent coarseness, tex[c]	14.8	4.1	3.9	9.3	1.5	0.9	2.9
Calculated coarseness, tex[c]	15.1	3.0	1.7	6.0	1.2	0.7	2.8
Apparent density, g/cm^3	0.38±0.06	0.54±0.05	1.67±0.26	0.56±0.07	0.67±0.11	0.63±0.10	1.58±0.25
Young's modulus, MPa	535±45	537±36	1786±320	361±67	564±114	425±133	1676±160
Specific modulus, MPa cm^3/g	1407±322	999±157	1064±355	646±199	863±323	664±312	1023±259
Tensile strength, MPa	16.5±4.4	25.5±3.9	57.0±19.5	9.7±3.2	14.9±4.5	14.2±6.0	67.4±18.3
Specific strength, MPa cm^3/g	43.4±17.8	47.4±11.5	34.0±16.9	17.3±7.9	22.8±10.8	22.1±12.8	41.1±17.6
Tenacity, cN/tex	4.34±0.52	4.74±0.31	3.40±0.64	1.73±0.36	2.28±0.30	2.21±0.59	4.12±0.47
Elongation at break, %	4.42±0.93	7.87±0.82	5.03±1.26	3.08±0.27	2.33±0.46	2.32±0.87	27.6±5.51

[a] Drawing ratio; i.e., ratio of winding speed to extrusion speed, both in m/min.

[b] Measured exceptionally with Axio Scope.A1 polarized light microscope (Zeiss, Germany)

[c] g/km

[d] Drawing ratio of CA

For water-coagulated CNF/CA, cross-sectional areas of the filament components were estimated assuming filament cross-section comprising two concentric rectangles: outer one with the dimensions measured for CNF/CA core/shell filament and inner one the dimensions of the CNF filament after CA shell removal. The inner rectangle was expected to be filled with CNF and the space between inner and outer rectangles with CA. Weight fractions of CNF and CA in a bicomponent filament were determined by weighing a batch of 0.1-0.3 g of filaments before and after removal of the shell. This was not possible for CNF/GG filaments given that shell removal would not be selective in this case, as both components disperse in the same solvents.

Total filament thickness, width and coarseness for systems with or without CA shell generally decrease with increasing DR. As the only exception, the thickness of the neat CNF filaments appeared to plateau at approximately 8 μm at DR of 5 and 9. This is probably related to the micrometer gauge approaching the limits of its resolution at such small thicknesses. This could also cause the unexpected development of the mass and volumetric ratios of CNF and CA in their drawn bicomponent filaments. At a DR of 9, the CNF/CA mass ratio (40:60, Figure S1a) becomes lower than their volumetric ratio (60:40, Figure S1b). Also, at a DR of 5, the CNF/CA mass ratio becomes exceptionally high (50:50, Figure S1a) and volumetric ratio exceptionally low (30:70, Figure S1b) compared to the other values of DR. Overall, the mass ratios obtained for CNF and CA (40-50 wt.% CNF : 50-60 wt.% of CA, Figure S1a) appear close to the CNF:CA mass ratio of 40:60 used in the dopes. The slight deviation probably arises from traces of CA left on the neat CNF filaments. In volume, the bicomponent filaments contained 30-60 vol-% of CNF and 40-70 vol-% of CA (Figure S1b).

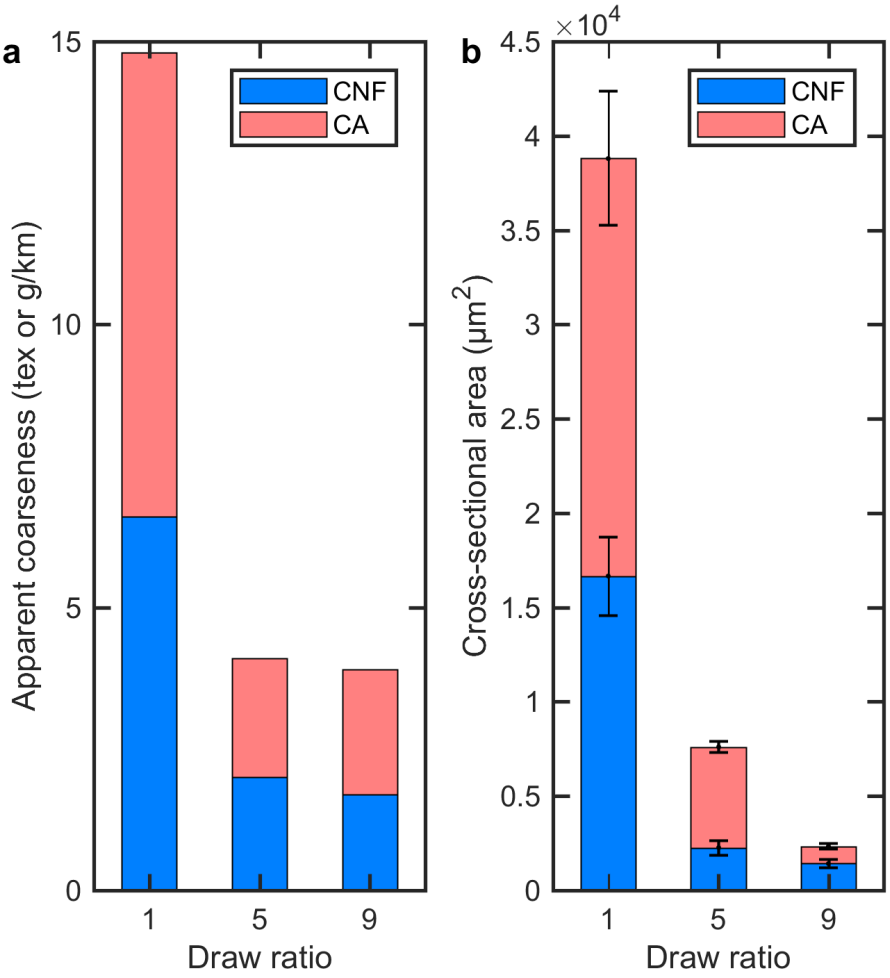

Figure S1. Effect of drawing on the linear density (a, corresponding to weight fractions) and cross-sectional area (b, corresponding to volume fractions) of the water-coagulated CNF/CA filament and its components. Error bars are defined as the standard deviation divided by the square root of the sample size (10 specimens). Spinning conditions: Tables S3, S4.

The increased DR also seems to produce denser filaments, at least in the case of those with CA shell retained. However, this densification with drawing is unlikely as pronounced as suggested by Table S6. For example, the 9-fold drawn filament has similar apparent coarseness to the 5-fold drawn (~4 tex), despite the clearly smaller dimensions. This leads to an artificially high apparent density of 1.67±0.26 g/cm^3, even though both the components alone have lower densities: CA 1.58±0.25 g/cm^3 (Table S6) and cellulose 1.5-1.6g/cm^3.[13] Moreover, manual measurement and weighing of filament pieces to obtain the apparent coarseness is of limited

resolution for light filaments. In fact, based on the extrusion and winding speeds as well as the solids content of the CNF and CA, a DR of 9 is expected to yield a core/shell filament with a calculated coarseness of only 1.7, which would correspond to a density of 0.73 g/cm^3. For the other filaments, the calculated coarseness matched closely the measured values (Table S6).

Stress-strain curves of the filaments with and without CA and drawing are presented in Figure S2. By increasing the DR, the strength and stiffness of the CNF/CA filaments augmented (Figure S2, purple). However, no clear effect of drawing was evident for neat CNF filaments (Figure S2, blue, inset). This indicates that the draw-induced strengthening of CNF/CA occurred mainly because of the contribution of the shell component and the draw did not significantly restructure the CNF inside the filament. Similarly, single-component filaments are known to be prone to tensile stress concentrating on the outer region of the filament, which coagulates first.[14] Because of the concentrated stress, this zone can develop a higher degree of orientation.[14] The dominant contribution of CA to the mechanical support of the bicomponent filament is corroborated by the higher strength and stiffness in the presence of CA compared to CNF alone (Table S6, Figure S2). This implies that the structure adopted by CNF enclosed by CA in a water bath is suboptimal for load-bearing but more useful for other purposes, such as water absorption, as discussed in the main article.

As the mechanical properties of the filament were calculated based on the physical properties, they are subject to error. For example, since the thinnest filament (DR 9) had a surprisingly high thickness of 7.7±0.3 μm (possibly due to limited resolution of the micrometer gauge), its real tensile strength may be higher than the reported 14.2±6.0 MPa. Considering this, the Young's modulus and tensile strength of CNF/CA filaments definitely seem to augment with drawing (Figure S2, Table S6). However, a different trend is observed for the values of specific modulus and strength as well as tenacity (Table S6). In fact, when normalizing the filament stiffness and strength against its coarseness instead of cross-sectional area, the strongest core/shell filament (DR 9) seems the weakest. This deviation arises from the questionably high apparent coarseness measured for this sample (Table S6). The trend observed for the Young's modulus and tensile strength normalized against the filament cross-sectional area can, therefore, be considered more reliable.

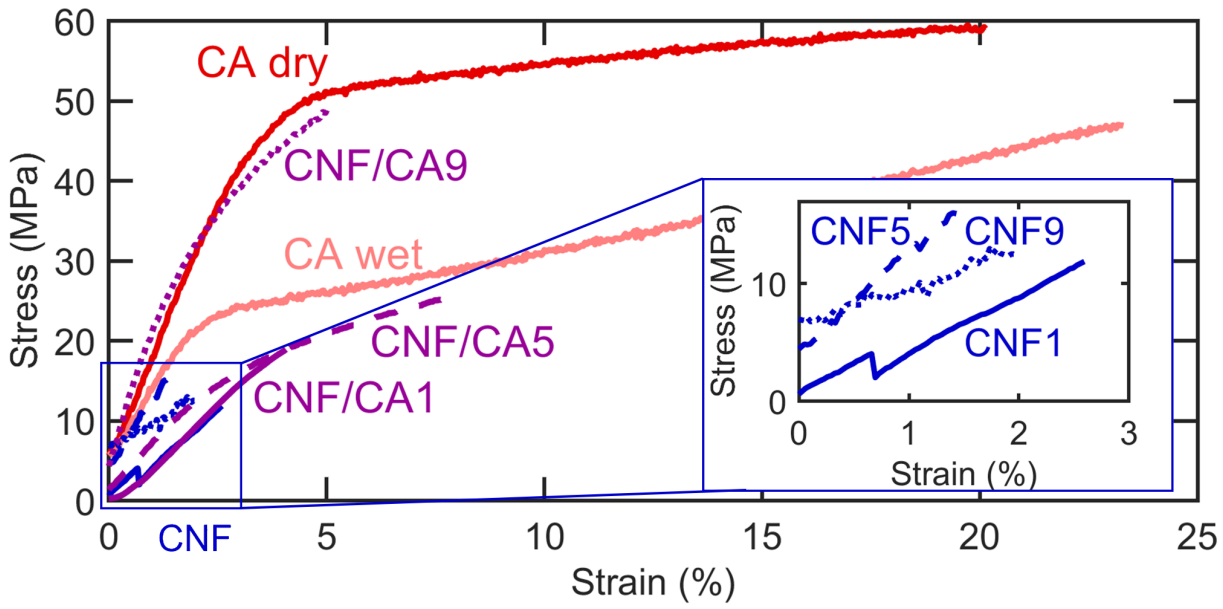

Figure S2. Representative stress-strain curves for filaments with the CA shell (CNF/CA, purple) and without it (CNF, blue) as well as the control with CA only (red). Numbers and line styles indicate the DR applied on CNF (1 – solid; 5 – dashed; 9 – dotted). Inset shows only the filaments after the shell removal. Spinning conditions: Tables S3, S4.

Nevertheless, the value of tenacity can be compared rather reliably, since it is independent of the filament cross-section and its fluctuations. The tenacity at varying DR (Table S6) indicate that single component CNF filaments produced at a DR of 5 presented the best performance. Also, the Young's modulus, specific modulus and specific strength peak at a DR of 5. This implies that, even if the drawing induced a slightly more load-bearing structure even in the CNF component, excess drawing may damage it.

Previously, CNF filaments have been subjected to drawing after drying while immersed in water[3] or acetone-water mixture,[6] capitalizing on the plasticizing effect of water.[15] By this "post-drawing" of a wood-based CNF filament under a DR of 1.3, the Young's modulus was increased from 8.2 to 33.7 GPa and the tensile strength from 118 to 289 MPa.[3] For a filament spun from bacterial cellulose, post-drawing (DR 1.2) increased the Young's modulus from 12 to 16.4 GPa and the tensile strength from 198 to 249 MPa.[6] Recently, a CNF-based filament was collected from an interface between dispersions of negatively charged CNF and a polycation, which formed a filament via inter-polyelectrolyte complexation.[16] When a DR of 1.2 was applied on

this type of bicomponent filament before complete drying, the Young's modulus increased from 15 GPa to 20-23 GPa and the tensile strength from 200 to 240-250 MPa, with the final values depending on the applied polyelectrolyte.[5]

Even though the core/shell spinning approach increased the maximum DR possible for wet-spun CNF, from the previously reported 1.3[3] to 9, no improvement in strength was measured upon drawing (Figure S2, inset). This might imply that an optimum DR value may exist for optimal filament performance, as indicated in the case of the post-drawn CNF filaments: increasing the DR from 1.2 to 1.3 failed to improve the tensile strength further above 289 MPa.[3] Such possible performance plateau with increasing DR has also been studied through simulations and flow focusing experiments at different extension rates.[17] When the extension rate was elevated, fibril orientation in a flow-focusing channel improved, though not as much as predicted through simulation. This led to the conclusion that increasing the extension on a CNF suspension also increases the resistance of the fibrils to orient.[17] A similar effect might cause the plateau observed at high extents of post-drawing and possibly also during core/shell spinning with drawing.

The effect of drawing on CNF restructuring can also be influenced by the extension rate. In post-drawing experiments, CNF filaments were stretched at extension rates ranging from 7.6×10^{-5} to 1.0×10^{-3} s^{-1}.[3,6] These are at least three decades lower than the lowest extension rates applied in the current core/shell spinning system. Possibly, the relaxation of CNF proceeds too slowly for the fibrils to react to the fast drawing. The hypothesis of a slow relaxation is supported by the increased alignment of CNF when the residence time of the hydrogel flowing in a needle was increased up to one minute.[18] Also, in rheometry determinations, the velocity profile of CNF (probably connected to hydrogel structure) has been shown to develop over approximately one minute.[19] However, we note that in these studies the CNF hydrogels were subjected to shear instead of extensional flow fields. Under extensional flow, the timescale of CNF alignment has been estimated to be ~0.31 s,[2] which implies that the CNF may react faster to extension than to shear. The slow relaxation, though, may be an advantage in certain cases, such as applications not requiring optimal fibril alignment but rather high porosity optimized by randomly oriented fibrils.

3. FILAMENT CRYSTALLINITY

The radial integrals of the 2D-WAXD patterns (Figure S3) show that all the CNF-containing filaments display the typical diffraction peaks for cellulose I crystallites at scattering vectors 12 and 15.8 nm^{-1}. When CNF was extruded in a GG shell, the peak at 15.8 nm^{-1} was accompanied by a shoulder at 14.4 nm^{-1}. This may originate from the contribution of crystallized GG, since the filament with GG only also has a peak at this position. As seen in the diffractogram of the neat CA filament, CA is mostly amorphous and thus invisible in the normalized radial integral of CNF and CA combined. Compared to the neat CNF filament, only a slight increase in the amorphous domain between the cellulose crystallite peaks can be observed for CNF/CA filament.

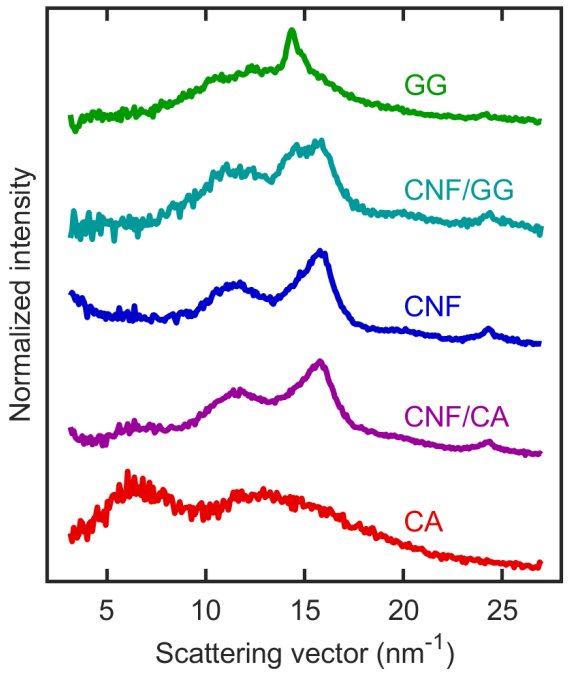

Figure S3. Radial integrals of the X-ray diffraction patterns of filaments coagulated for 5 min in ethanol, apart from GG (5 min in acetone) and CA (fast in water). Spinning conditions: CA – Tables S3, S4; others – Table S1.

4. EFFECT OF THE SHELL MATERIAL AND COAGULATION SYSTEM ON FILAMENT PROPERTIES

Physical-mechanical properties of the core/shell filaments spun with different material combinations and coagulation systems are compiled in Table S7. The extrusion speeds and solids content of the precursor dopes mostly determine the filament weight and dimensions. The thinnest and lightest filaments were obtained by extruding only GG (solids content 1 wt.%) at a speed of 3 ml/min. Larger and heavier filaments were spun when changing to CNF (solids content 1.5 wt.%) and adding a GG shell at a speed of 1 ml/min. The maximum dimensions and coarseness resulted from a similar CNF flow combined with a three times slower but 15 times more concentrated CA flow. Surprisingly, when removing the CA from this sample to obtain neat CNF filaments, a large width results, deviating from the trend. This implies that the drying and shell removal procedures flatten the CNF core even more heavily than the whole core/shell filament. Thus, even though the filament has an apparent coarseness of 20.7 tex (approx. one third of its precursor filament with both CNF and CA), this material is spread over a heavily flattened cross-section. As the apparent coarseness and density for this filament are low but it still maintains a fairly high load-bearing capacity, it has a remarkably high tenacity of 9.37±0.6 cN/tex in comparison to the other samples.

Table S7. Physical-mechanical properties of the filament samples in dry state. Error margins are defined as the standard deviation divided by the square root of the sample size (5 specimens, unless stated otherwise). Spinning conditions: Table S1.

Coagulant	Ethanol			Acetone	
Components	CNF[c]	CNF/CA	CNF/GG	CNF/GG	GG
Apparent thickness, μm[a]	81±10	135±9	167±5	93±2	59±6
Apparent width, μm[a]	608±33	599±53	353±30	424±54	251±25
Apparent coarseness, tex[b]	20.7	60.3	35.5	35.0	14.0
Calculated coarseness, tex[b]	5.5	280.3	23.9	23.9	3.7
Apparent density, g/cm^3 [a]	0.42±0.08	0.75±0.11	0.60±0.07	0.89±0.13	0.95±0.19
Young's modulus, MPa	1103±75	907±85	1313±122	2074±121	609±200[d]
Specific modulus, MPa cm^3/g	2623±659	1216±298	2178±460	2340±491	644±338[d]
Tensile strength, MPa	39.4±10.0	29.9±7.5	38.0±9.9	69.5±15.7	11.6±5.3[d]
Specific strength, MPa cm^3/g	93.7±40.8	40.0±16.2	63.0±23.8	78.4±29.6	12.3±8.0[d]
Tenacity, cN/tex	9.37±0.6	4.01±0.41	6.30±0.90	7.84±0.58	1.23±0.32[d]
Elongation at break, %	8.34±1.16	5.51±0.47	5.42±0.49	6.24±0.49	2.45±0.43[d]

[a] sample size 10 specimens

[b] g/km

[c] Spun with a CA shell, which was removed afterwards

[d] Sample size 3 specimens

5. FILAMENT INTERACTIONS WITH WATER

Wet mechanical properties are summarized in Table S8. The behaviors in wet state are explained by the water absorption capacities (Figure 4b) and water contact angles on the filament materials (Figure S4), as discussed in the main article. Porosity is expected to pay an essential role in filament-water interactions.

All filaments comprising CNF only had an apparent density below 0.8 g/cm^3, even though the real density might have been slightly higher for the one drawn at a DR of 9, as described earlier. For a cellulosic material, a density below 0.8 g/cm^3 corresponds to a porosity of more than 50% (based on the density of pure crystalline cellulose of 1.5-1.6 g/cm^3).[13] This suggests that the core/shell spinning produces more porous CNF filaments than the 10%[22] or up to 32%[23] reported in earlier studies using a single needle for spinning of pure CNF.

Table S8. Mechanical properties of core/shell filaments after soaking in water over-night. Error margins are defined as the standard deviation divided by the square root of the sample size (5 specimens, unless stated otherwise). Spinning conditions: CA – Tables S3, S4; others – Table S1.

Coagulant	Ethanol			Acetone	Water
Components	CNF[a,b]	CNF/CA	CNF/GG[b]	CNF/GG	CA
Wet Young's modulus, MPa	18±6	123±11	35±10	81±6	755±124
% of dry modulus	2	14	3	4	45
Wet tensile strength (MPa)	0.55±0.17	2.94±0.62	0.64±0.22	2.70±0.59	40.02± 9.7
% of dry strength	1	10	2	4	59
Wet tenacity, cN/tex	0.13±0.02	0.39±0.02	0.11±0.02	0.30±0.02	2.44±0.21
Wet elongation at break, %	2.42±0.62	3.71±0.50	1.51±0.02	4.97±0.91	22.53±4.60

[a] Spun with a CA shell, which was removed afterwards.

[b] Sample size 2

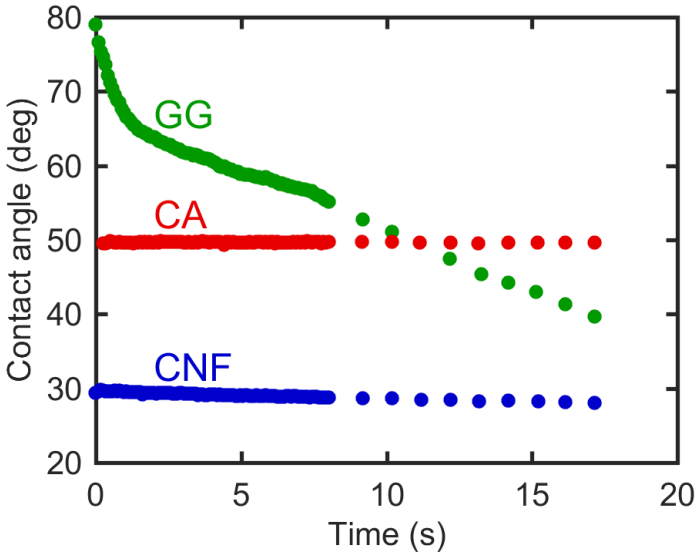

Figure S4. Development of water contact angle over time on films cast from the spinning dopes.

6. EFFECT OF CORE/SHELL SYSTEM ON SPINNABILITY

Essentially, infinite length of filament could be spun via the CNF/CA system, even incorporating drawing, since the shell prevents the breaking of the wet filament. Furthermore, this system expanded the spinnability range of CNF, allowing for spinning even at a solids content as low as 1 wt.%, which would not form recoverable filaments otherwise. When changing to GG as a shell, though, long filament could be obtained only from CNF if used at a minimum solids content of 1.5 wt.%. Both shell materials could be spun as a single component or alone (control filaments). CA could even be spun continuously and with drawing, as already well established.[20]

The combination of CNF and GG also allowed spinning of long filaments without breaking. However, such filaments could be spun continuously only when collected by a conveyor belt (Figure 1c), since the filament was not strong enough for pick up from the bath through air, unless several minutes of immersion were allowed. This implies that the coagulation proceeds more slowly for GG (order of minutes) than for CA (order of seconds). Moreover, the CNF/GG filament could not be consistently drawn while coagulating, apart from the small amount of drawing that naturally occurs during winding and drying. During the winding, the gravity pulls the filament downwards while the winder pulls it upwards; and during the drying, the filament

tends to contract because of the solvent depletion. The winder restricts the contraction induced by drying, leading to a drawing effect.

Large batches of filament were obtained by optimizing the production speed. Using a larger prototype spinning line (Figure 1b) allowed an increased production rate of CNF/CA filaments, up to 33 m/min, applying the spinning conditions specified in Table S2. Even for the CNF/GG system, adjusting the spinning line with a supportive conveyor belt (Figure 1c) enabled a production speed of up to 1.2 m/min. However, this setup only allows for approximately 3 s of coagulation for CNF and 16 s for GG, considering that a filament element in the core travels through a distance of 24 cm at an average speed of 4.7 m/min, while a shell element covers the same distance at an average speed of 0.9 m/min (Table S2).

The quality of the CNF/GG filaments was seemingly improved by spinning right after re-filling the coagulation bath as full as possible. Filaments spun in a fresh and full coagulation bath appeared both rounder (less flattened) and able to bear more load. Thereafter, the filaments became increasingly brittle when spun to a coagulant that had already been somewhat diluted with water after extended extrusion operation. This phenomenon can be explained by approximating the speed of the coagulation induced by the diffusion of the coagulant into the filament according to Equation S2[21]

$$coagulation\ speed = \frac{W^2(t)}{t} = \frac{VD_{in}c}{\pi LR^2} \quad \text{(S2)}$$

where W is the thickness of the coagulated layer below the surface of the filament; V is the volume of the coagulant in the bath; D_{in} is the diffusion coefficient of the coagulant into the solvent in the dope; c is the volumetric concentration of the coagulant in the solvent right below the filament surface; L is the length of the studied filament section and R is the filament radius.

Equation S2 shows that increasing the total volume of the coagulant and/or its concentration below the filament surface increase the coagulation speed. During spinning, both of these effects are counteracted, as the coagulant keeps evaporating and diluting due to the incoming flux of the dope solvent. Thus, for optimal spinning conditions a large coagulation bath with purge and make up system would be ideal.

REFERENCES

(1) Lundahl, M. J.; Berta, M.; Ago, M.; Stading, M.; Rojas, O. J. Shear and Extensional Rheology of Aqueous Suspensions of Cellulose Nanofibrils for Biopolymer-Assisted Filament Spinning. *Manuscript Submitted to Biomacromolecules* **2018**.

(2) Håkansson, K. M. O.; Fall, A. B.; Lundell, F.; Yu, S.; Krywka, C.; Roth, S. V; Santoro, G.; Kvick, M.; Prahl Wittberg, L.; Wågberg, L.; Söderberg, L. D. Hydrodynamic Alignment and Assembly of Nanofibrils Resulting in Strong Cellulose Filaments. *Nat. Commun.* **2014**, *5*, 4018.

(3) Torres-Rendon, J. G.; Schacher, F. H.; Ifuku, S.; Walther, A. Mechanical Performance of Macrofibers of Cellulose and Chitin Nanofibrils Aligned by Wet-Stretching: A Critical Comparison. *Biomacromolecules* **2014**, *15*, 2709–2717.

(4) Kafy, A.; Kim, H. C.; Zhai, L.; Kim, J. W.; Hai, L. Van; Kang, T. J.; Kim, J. Cellulose Long Fibers Fabricated from Cellulose Nanofibers and Its Strong and Tough Characteristics. *Sci. Rep.* **2017**, *7*, 17683.

(5) Toivonen, M. S.; Kurki-Suonio, S.; Wagermaier, W.; Hynninen, V.; Hietala, S.; Ikkala, O. Interfacial Polyelectrolyte Complex Spinning of Cellulose Nanofibrils for Advanced Bicomponent Fibers. *Biomacromolecules* **2017**, *18*, 1293–1301.

(6) Yao, J.; Chen, S.; Chen, Y.; Wang, B.; Pei, Q.; Wang, H. Macrofibers with High Mechanical Performance Based on Aligned Bacterial Cellulose Nanofibers. *ACS Appl. Mater. Interfaces* **2017**, *9*, 20330–20339.

(7) Shen, Y.; Orelma, H.; Sneck, A.; Kataja, K.; Salmela, J.; Qvintus, P.; Suurnäkki, A.; Harlin, A. High Velocity Dry Spinning of Nanofibrillated Cellulose (CNF) Filaments on an Adhesion Controlled Surface with Low Friction. *Cellulose* **2016**, *23* (6), 3393–3398.

(8) Rahman, M. M.; Netravali, A. N. Aligned Bacterial Cellulose Arrays as "Green" Nanofibers for Composite Materials. *ACS Macro Lett.* **2016**, *5*, 1070–1074.

(9) Rahman, M. M.; Netravali, A. N. High-Performance Green Nanocomposites Using Aligned Bacterial Cellulose and Soy Protein. *Compos. Sci. Technol.* **2017**, *146*, 183–190.

(10) Tang, H.; Butchosa, N.; Zhou, Q. A Transparent, Hazy, and Strong Macroscopic Ribbon of Oriented Cellulose Nanofibrils Bearing Poly(Ethylene Glycol). *Adv. Mater.* **2015**, *27*, 2070–2076.

(11) Sehaqui, H.; Ezekiel Mushi, N.; Morimune, S.; Salajkova, M.; Nishino, T.; Berglund, L. A. Cellulose Nanofiber Orientation in Nanopaper and Nanocomposites by Cold Drawing. *ACS Appl. Mater. Interfaces* **2012**, *4* (2), 1043–1049.

(12) Baez, C.; Considine, J.; Rowlands, R. Influence of Drying Restraint on Physical and Mechanical Properties of Nanofibrillated Cellulose Films. *Cellulose* **2014**, *21* (1), 347–356.

(13) Dufresne, A. Nanocellulose: A New Ageless Bionanomaterial. *Mater. Today* **2013**, *16* (6), 220–227.

(14) Ziabicki, A. *Fundamentals of Fibre Formation*; John Wiley & Sons: London, 1976.

(15) Benítez, A. J.; Torres-Rendon, J.; Poutanen, M.; Walther, A. Humidity and Multiscale Structure Govern Mechanical Properties and Deformation Modes in Films of Native Cellulose Nanofibrils. *Biomacromolecules* **2013**, *14* (12), 4497–4506.

(16) Grande, R.; Trovatti, E.; Carvalho, A. J. F.; Gandini, A. Continuous Microfiber Drawing by Interfacial Charge Complexation between Anionic Cellulose Nanofibers and Cationic Chitosan. *J. Mater. Chem. A* **2017**, *00*, 1–6.

(17) Hakansson, K. M. O.; Lundell, F.; Prahl-Wittberg, L.; Söderberg, L. D. Nanofibril Alignment in Flow Focusing: Measurements and Calculations. *J. Phys. Chem. B* **2016**, *120* (27), 6674–6686.

(18) Mohammadi, P.; Toivonen, M. S.; Ikkala, O.; Wagermaier, W.; Linder, M. B. Aligning Cellulose Nanofibril Dispersions for Tougher Fibers. *Sci. Rep.* **2017**, *7*, 11860.

(19) Martoïa, F.; Perge, C.; Dumont, P. J. J.; Orgéas, L.; Fardin, M. A.; Manneville, S.; Belgacem, M. N. Heterogeneous Flow Kinematics of Cellulose Nanofibril Suspensions under Shear. *Soft Matter* **2015**, *11*, 4742–4755.

(20) Dickie, W. A.; Sowter, P. F. C. Production of Artificial Filaments, Films, and like Materials. US2147641A, 1929.

(21) Tripathi, A.; Rutkevičius, M.; Bose, A.; Rojas, O. J.; Khan, S. A. Rational Design Principles for Production of Porous Polymer Fiber during Wet-Spinning. *Manuscr. under Prep.* **2018**.

(22) Walther, A.; Timonen, J. V. I.; Díez, I.; Laukkanen, A.; Ikkala, O. Multifunctional High-Performance Biofibers Based on Wet-Extrusion of Renewable Native Cellulose Nanofibrils. *Adv. Mater.* **2011**, *23*, 2924–2928.

(23) Lundahl, M. J.; Cunha, A. G.; Rojo, E.; Papageorgiou, A. C.; Rautkari, L.; Arboleda, J. C.; Rojas, O. J. Strength and Water Interactions of Cellulose I Filaments Wet-Spun from Cellulose Nanofibril Hydrogels. *Sci. Rep.* **2016**, *6*, 30695.